Experimental determination of ground-state correlation effects in molecular nitrogen

Ronaldo S. Barbieri and R. A. Bonham
Department of Chemistry, Indiana University, Bloomington, Indiana 47405
(Received 11 July 1991)

High-energy (25–28-keV) electron-impact spectroscopy (HEEIS) has been used to measure a relatively complete Bethe surface for molecular nitrogen. This surface, placed on an absolute scale by Bethe-sum-rule normalization of the generalized oscillator strength (GOS), has been employed to obtain the x-ray incoherent scattering factor $S(K)$ as a function of the momentum transfer K by use of a sum rule of the GOS. Ground-state correlation effects on $S(K)$ were obtained by comparing the experimental results with theory based on a near-Hartree-Fock molecular wave function. The results are compared with recent theoretical calculations of valence-shell correlation effects. It is argued that x-ray and electron-scattering experiments offer the most sensitive tests currently available for valence-shell electron-correlation effects in the ground electronic states of molecules. The results obtained coupled with available theory suggest that correlation effects on the one-electron density play a dominant role in the determination of the total correlation energy of the nitrogen molecule.

PACS number(s): 34.80.Gs, 33.90.+h, 35.80.+s

I. INTRODUCTION

The aim of this paper is to demonstrate how very sensitive information on electron-correlation effects in the ground states of atoms and molecules can be obtained by experiment. While various spectroscopic and photoionization processes reveal the effects of electron correlation on the ground-state structure of an atom or molecule the interpretation of such information involves a detailed knowledge of the excited state [1]. Hence such experiments do not normally lead to unambiguous information on the ground state. The so-called $(e,2e)$ experiments are similar to the photoionization case in this regard. The orbital momentum density shows little sensitivity to electron correlation [2] as does the total momentum density measured in Compton scattering experiments [3]. Shakeup and shakeoff features in $(e,2e)$ spectroscopy can be very sensitive to correlation [4] but again their interpretation involves a knowledge of excited states, which only complicates the analysis. Certain $(\gamma,2e)$ and $(e,3e)$ angular correlation studies have been proposed [5–11] which would directly measure the second-order density matrix in momentum space and could presumably be very sensitive to ground-state correlation effects. So far only a few successful experiments of this type have been carried out [9–11]. This leaves only the classical scattering approaches initiated in the 1920s [12] which have not been as successful as originally hoped because of the experimental difficulties involved in measuring accurate absolute scattered intensities. It has only been possible to realize the potential of the classical approach with the advent of modern technology [13]. Recent works have focused on elastic electron scattering [14], total electron inelastic scattering [15], and total, elastic plus inelastic, x-ray scattering [16]. The elastic scattered intensity can be related to the Fourier transform of the diagonal one-electron density matrix or the electron density $\rho(\mathbf{r})$ [17], which has been thought to be rather insensitive to electron correlation [18] but very sensitive to electron bond formation effects in molecules [19]. The inelastic scattering, on the other hand, can be employed to obtain the generalized oscillator strength (GOS), which through well-known sum rules can be used to calculate the x-ray incoherent scattering factor [20] which is simply related to the electron pair correlation function and is, as it has been shown, a very correlation-sensitive quantity [15]. The connection between these experiments and the various charge densities is made by use of first Born type scattering theories [13,21]. The validity of using the Born approximation can be subjected to experimental test and confirmed within the experimental uncertainties involved [14]. In this paper the focus will be on experimental determination of the x-ray incoherent scattering factor for molecular nitrogen by use of a sum rule of the GOS [15].

II. THEORY

The connection between inelastic scattering and the electron pair correlation function via a sum rule of the GOS for the case of molecules is not well known [22–24] and it is therefore worthwhile to present the details here. For the molecular case the GOS, which is an experimental observable, is defined for excitations into the continuum as [24]

$$\frac{df(K(E),E)}{dE}=\sum_{\nu}\delta(E-E_{\nu})E_{\nu}\left|\left\langle\Psi_0\left|\sum_{n=1}^{M}Z_n e^{i\mathbf{K}\cdot\mathbf{R}_n}-\sum_{i=1}^{N}e^{i\mathbf{K}\cdot\mathbf{r}_i}\right|\Psi_{\nu}\right\rangle\right|^2\Big/K(E)^2 \tag{1a}$$

or

$$f(K(E_\nu),E_\nu)=E_\nu\left|\left\langle\Psi_0\left|\sum_{n=1}^{M}Z_n e^{i\mathbf{K}\cdot\mathbf{R}_n}-\sum_{i=1}^{N}e^{i\mathbf{K}\cdot\mathbf{r}_i}\right|\Psi_\nu\right\rangle\right|^2\Big/K(E_\nu)^2 \tag{1b}$$

for discrete excitation processes where $\mathbf{K}$ is the momentum transfer and E is the energy loss with both $\mathbf{K}$ and E in Rydberg atomic units. In Eq. (1a) the sum over ν runs over all states accessible to excitation with an energy transfer (loss) E from a projectile electron. The positions of the M nuclei and N electrons of the target molecule are given by $\mathbf{R}_n$ and $\mathbf{r}_i$, respectively, with Z_n the atomic number of the nth nucleus. The sums over n and i will be omitted for brevity but understood in what follows. The nonvanishing of the term $Z_n e^{i\mathbf{K}\cdot\mathbf{R}_n}$ in the molecular case is the result of the wave-function dependence on the nuclear motion.

The sum rules of the GOS are defined generally as

$$S(l,\bar{K})=\sum_\nu E_\nu^l f(\bar{K},E_\nu)+\int_{E_i}^{\infty}dE\,E^l\frac{df(\bar{K},E)}{dE} \tag{2}$$

where E_i is the lowest ionization potential and the sum over ν is over all possible discrete excitations. Note that the energy-loss range must be extended up to infinity and measurements must be carried out at a constant momentum transfer $\bar{K}$. The sum rules of interest to this work are $l=0$, called the Bethe sum rule [20], which is used for normalization of the data to an absolute scale and the $l=-1$ sum rule which yields the desired result. The sums involved for $l=0$ and -1 can be evaluated exactly in terms of known constants or ground-state expectation values as [23,24]

$$S(0,\bar{K})=N+\sum_{n=1}^{M}Z_n^2/(1836M_n) \tag{3}$$

with M_n the mass of the nth nucleus in amu's and [22,24]

$$S(-1,\bar{K})=(\langle\Psi_0||Z_n e^{i\bar{\mathbf{K}}\cdot\mathbf{R}_n}-e^{i\bar{\mathbf{K}}\cdot\mathbf{r}_i}|^2|\Psi_0\rangle - |\langle\Psi_0|Z_n e^{i\bar{\mathbf{K}}\cdot\mathbf{R}_n}-e^{i\bar{\mathbf{K}}\cdot\mathbf{r}_i}|\Psi_0\rangle|^2)/\bar{K}^2 . \tag{4}$$

Equation (4) can be rearranged by adding and subtracting the term $\langle\Psi_{\rm VRT}||F(\bar{\mathbf{K}})|^2|\Psi_{\rm VRT}\rangle$ where the average is over the vibrational-rotational-translational (VRT) motion of the molecule and $F(\bar{\mathbf{K}})$ is the electronic molecular x-ray coherent scattering factor defined as

$$F(\bar{\mathbf{K}})=\langle\Psi_E|e^{i\bar{\mathbf{K}}\cdot\mathbf{r}_i}|\Psi_E\rangle$$

where Ψ_E is the ground-electronic-state Born-Oppenheimer wave function [17]. The result, after some algebra, can be written as

$$\begin{aligned}S(-1,\bar{K})\bar{K}^2=N&+\langle\Psi_0|e^{i\bar{\mathbf{K}}\cdot\mathbf{r}_{ij}}|\Psi_0\rangle_{i\neq j}-\langle\Psi_{\rm VRT}||F(\bar{\mathbf{K}})|^2|\Psi_{\rm VRT}\rangle\\&+[\langle\Psi_0|Z_nZ_m e^{-i\bar{\mathbf{K}}\cdot\mathbf{R}_{nm}}-Z_n e^{i\bar{\mathbf{K}}\cdot(\mathbf{R}_n-\mathbf{r}_i)}-Z_m e^{-i\bar{\mathbf{K}}\cdot(\mathbf{R}_m-\mathbf{r}_i)}|\Psi_0\rangle\\&+\langle\Psi_{\rm VRT}||F(\bar{\mathbf{K}})|^2|\Psi_{\rm VRT}\rangle-|\langle\Psi_0|Z_n e^{i\bar{\mathbf{K}}\cdot\mathbf{R}_n}-e^{i\bar{\mathbf{K}}\cdot\mathbf{r}_i}|\Psi_0\rangle|^2] .\end{aligned} \tag{5}$$

Note that Eq. (5) is exact and that the first three terms on the right of the equal sign are identical to the definition of the x-ray incoherent factor for atoms [13,20], $S(\bar{K})$, except that Ψ_0 is the exact ground-state molecular wave function and averages over VRT motion are included. If we invoke the Born-Oppenheimer approximation for Ψ_0 in those terms in the square brackets then Ψ_0 can be replaced by the product $\Psi_{\rm VRT}\Psi_E$. This reduces the terms in the brackets, which we denote as $S(\bar{K})_{\rm VRT}$, to

$$S(\bar{K})_{\rm VRT}=\langle\Psi_{\rm VRT}||Z_n e^{i\bar{\mathbf{K}}\cdot\mathbf{R}_n}-F(\bar{\mathbf{K}})|^2|\Psi_{\rm VRT}\rangle - |\langle\Psi_{\rm VRT}|Z_n e^{i\mathbf{K}\cdot\mathbf{R}_n}-F(\bar{\mathbf{K}})|\Psi_{\rm VRT}\rangle|^2 \tag{6}$$

where $S(\bar{K})_{\rm VRT}$ can be recognized as the difference between the elastic line intensity including averages over all possible VRT excitations that leave the molecule in its ground electronic state and the intensity for elastic scattering obtained using an energy analyzer with infinite energy resolution [24]. The average over VRT in the last term on the right represents the weighted sum of elastic scattering from all initially excited states of the molecule. If the elastic line, including all important VRT excitations of the ground electronic state, is well separated experimentally from the electronically excited states and their VRT excitations then we may omit the elastic line from our analysis and use the atomiclike sum rule

$$S(-1,\bar{K})\bar{K}^2=N+\langle\Psi_0|e^{i\bar{\mathbf{K}}\cdot\mathbf{r}_{ij}}|\Psi_0\rangle_{i\neq j}-\langle\Psi_{\rm VRT}||F(\bar{\mathbf{K}})|^2|\Psi_{\rm VRT}\rangle \tag{7}$$

with Ψ_0 being the exact ground-state wave function. Assuming that the VRT motion is separable as $\Psi_{\rm VRT}=\Psi_V\Psi_R\Psi_T$ and if Ψ_0 is replaced by $\Psi_V\Psi_R\Psi_T\Psi_E$ then Eq. (7) can be written as [25,26]

$$S_I(-1,\bar{K})\bar{K}^2=\left\langle\Psi_V\Psi_T\left|\frac{1}{4\pi}\int d\Omega_{\bar{\mathbf{K}}}[N+\langle\Psi_E|e^{i\bar{\mathbf{K}}\cdot\mathbf{r}_{ij}}|\Psi_E\rangle_{i\neq j}-|F(\bar{\mathbf{K}})|^2]\right|\Psi_T\Psi_V\right\rangle \tag{8}$$

where the terms in the square brackets constitute an x-ray incoherent scattering factor for a molecule in a fixed orientation in space. This result is then averaged over all spatial orientations [25], $\int d\Omega_{\bar{K}}$, and over the vibrational and translational motion [24]. The subscript I has been appended to the sum rule to indicate that the elastic line has been excluded from the analysis. We believe that Eq. (8) is sufficiently accurate to use as a comparison model with the results of experiment. A similar argument can be made to justify use of the Bethe sum rule for atoms for the molecular case since the molecular correction is only 0.03 to the atomic value of the sum rule which is 14 in the case of N_2.

The connection between Eq. (8) and the electron pair correlation function can be established by carrying out the rotational averaging and by integrating over all electronic coordinates except those for electrons 1 and 2 with the result

$$S_I(\bar{K})=S_I(-1,\bar{K})\bar{K}^2$$
$$=\left\langle \Psi_V\Psi_T \left| N+\int_0^\infty dr_{12}P_0(r_{12})\frac{\sin\bar{K}r_{12}}{\bar{K}r_{12}}-\int d\mathbf{r}_1\rho(\mathbf{r}_1)\int d\mathbf{r}_2\rho(\mathbf{r}_2)\frac{\sin\bar{K}r_{12}}{\bar{K}r_{12}} \right| \Psi_V\Psi_P \right\rangle \tag{9}$$

where $P_0(r_{12})$ is the electron pair correlation function and $\rho(\mathbf{r})$ is the three-dimensional one-electron density for the molecule. Both these densities depend on the nuclear position vectors $\mathbf{R}_n$ with their directions referred to the principal axis coordinate system of the molecule [26]. The electron pair correlation function can be defined in terms of the diagonal second-order density matrix [17], $\Gamma(\mathbf{R}_n,\mathbf{r}_1,\mathbf{r}_2;\mathbf{r}_1,\mathbf{r}_2,\mathbf{R}_n)$, as

$$P(\mathbf{r}_{12},\mathbf{R}_n)=r_{12}^2\int d\mathbf{r}_2\Gamma(\mathbf{R}_n,\mathbf{r}_2+\mathbf{r}_{12},\mathbf{r}_2;\mathbf{r}_2+\mathbf{r}_{12},\mathbf{r}_2,\mathbf{R}_n) \tag{10}$$

which is normalized to $N(N-1)$ with N the number of electrons in the molecule. Note that we have defined $P(\mathbf{r}_{12},\mathbf{R}_n)$ in terms of the Born-Oppenheimer ground-state wave function in keeping with our choice of Eq. (8) as the vehicle for experimental interpretation. The function $P_0(r_{12})$ used in Eq. (9) is just $P(\mathbf{r}_{12},\mathbf{R}_n)$ averaged over all orientations of $\mathbf{r}_{12}$ with respect to the principal axis coordinate system of the molecule with the dependence on $\mathbf{R}_n$ suppressed. The electron pair correlation function is the s wave term in a spherical harmonic expansion of $P(\mathbf{r}_{12},\mathbf{R}_n)$ in terms of the orientation angles of $\mathbf{r}_{12}$ with respect to the principal axis system and corresponds physically to the radial probability for finding any two electrons in the molecule separated by a distance r_{12}. The one-electron density $\rho(\mathbf{r})$ is the diagonal one-electron density matrix for the Born-Oppenheimer wave function for the ground electronic state and is normalized to $N=14$ [17]. The dependence of $\rho(\mathbf{r})$ on $\mathbf{R}_n$ has been omitted and is to be understood. If the transformations $\mathbf{r}_{12}=\mathbf{r}_1-\mathbf{r}_2$ and $\mathbf{R}=(\mathbf{r}_1+\mathbf{r}_2)/2$ are made in the last term on the right of Eq. (9) then the quantity $S_I(\bar{K})-N$ can be written as a Fourier transform of the difference between two-electron pair correlation functions as

$$S_I(\bar{K})-N=\left\langle \Psi_V\Psi_T \left| \int_0^\infty dr_{12}[P_0(\mathbf{r}_{12})-P_0^{\rm cl}(r_{12})]\frac{\sin\bar{K}r_{12}}{\bar{K}r_{12}} \right| \Psi_T\Psi_V \right\rangle$$
$$=\int_0^\infty dr_{12}[\bar{P}_0(r_{12})-\bar{P}_0^{\rm cl}(r_{12})]\frac{\sin\bar{K}r_{12}}{\bar{K}r_{12}} \tag{11}$$

where $P_0^{\rm cl}(r_{12})$ is a classical electron pair correlation function defined as

$$P_0^{\rm cl}(r_{12})=r_{12}^2\int d\Omega_{\mathbf{r}_{12}}\int d\mathbf{R}\,\rho\left[\mathbf{R}+\frac{\mathbf{r}_{12}}{2}\right]\rho\left[\mathbf{R}-\frac{\mathbf{r}_{12}}{2}\right]$$
$$=(2/r_{12}\pi)\int_0^\infty dK'K'\left[\frac{1}{4\pi}\int d\Omega_{\mathbf{K}'}|F(\mathbf{K}')|^2\right]\sin K'r_{12} \tag{12}$$

and the bar over the P's signifies that the pair correlation functions are VT averaged. The quantity in the large parentheses in Eq. (12) is the x-ray elastic scattering averaged over all rotational excitations [25]. Hence the difference between the quantum electron pair correlation function for the molecule and its classical counterpart, averaged over the VT motion in the ground state, can be calculated directly from the experiment by Fourier transformation.

Additional information about the target molecule ground state can be obtained by expanding $S_I(\bar{K})-N$ in powers of $\bar{K}$ in the limit as $\bar{K}$ goes to zero and in the limit as $\bar{K}$ goes to infinity. As $\bar{K}$ goes to zero [27,28]

$$\lim_{K\to 0}[S_I(\bar{K})-N]=-N-(\bar{K}^2/6)\int_0^\infty dr_{12}[\bar{P}_0^{\rm cl}(r_{12})-\bar{P}_0(r_{12})]r_{12}^2+O(\bar{K}^4)$$
$$=-N+\frac{\bar{K}^2}{3}[\langle r^2\rangle+\langle r_1r_2\cos\theta_{12}\rangle-(\boldsymbol{\mu}_e\cdot\boldsymbol{\mu}_e)]+O(\bar{K}^4) \tag{13}$$

where $\langle r^2\rangle=\sum_{i=1}^{N}\langle r_i^2\rangle$ is the average square radius of the molecule [29],

$$\langle r_1 r_2\cos\theta_{12}\rangle=\sum_{\substack{i\\ i\neq j}}\sum_{j}\langle \mathbf{r}_i\cdot\mathbf{r}_j\rangle$$

is a two-electron expectation value which should be especially sensitive to angular correlations between the electrons [30], and μ_e is the electronic component of the permanent dipole moment of the molecule. Note that all expectation values are VT averaged. We may define an effective average interelectronic angle $\langle\cos\theta_{12}\rangle$ as

$$\langle\cos\theta_{12}\rangle=\sum_{\substack{j=1\\ j=1}}^{N}\sum_{j=1}^{N}\langle \mathbf{r}_i\cdot\mathbf{r}_j\rangle\Big/\sum_{i=1}^{N}\langle r_i^2\rangle \tag{14}$$

after Krause, Morgan, and Berry [30] who defined a similar effective correlation angle related to the $\langle \mathbf{p}_1\cdot\mathbf{p}_2\rangle$ expectation value of the target electron's momenta $\mathbf{p}_1$ and $\mathbf{p}_2$ according to

$$\langle\cos\theta_{12}\rangle=\frac{\langle \mathbf{p}_1\cdot\mathbf{p}_2\rangle}{\langle T\rangle}\ , \tag{15}$$

where $\langle T\rangle$ is the electronic kinetic energy. One can also obtain $\langle\cos\theta_{12}\rangle$ defined in Eq. (15) from inelastic scattering experiments. The $S_I(1,\bar{K})$ sum rule, which depends critically on accurate determination of the high-energy loss tail of the GOS, provides such a connection as can be seen through the relation [20]

$$\lim_{K\to 0}S_I(1,\bar{K})=S(1)=2\left[\sum_{j}\langle \mathbf{p}_j^2\rangle+\sum_{\substack{j\\ j\neq k}}\sum_{k}\langle \mathbf{p}_j\cdot\mathbf{p}_k\rangle\right] \tag{16}$$

where the first term in the large parentheses is the absolute value of the total energy according to the virial theorem while the second term is the one that carries electron-correlation information [31].

In the limit as $\bar{K}$ goes to infinity, $S_I(\bar{K})-N$ can be written as [32,33]

$$\begin{aligned}S_I(\bar{K})-N&=-(2/\bar{K}^4)\frac{d[\bar{P}_0(r_{12})/r_{12}^2]}{dr_{12}}\bigg|_{r_{12}=0}+O(1/\bar{K}^6)\\&=(2/\bar{K}^4)\lim_{r_{12}\to 0}[\bar{P}_0(r_{12})/r_{12}^2]+O(1/\bar{K}^6)\\&=(2/\bar{K}^4)\bar{h}(0)+O(1/\bar{K}^6)\end{aligned} \tag{17}$$

where the last result, due to Thakkar and Smith [33], is valid as long as the ground state of the molecule is nondegenerate. Equation (17) comes from the cusp condition for the intracule density, $h(r_{12})=P_0(r_{12})/r_{12}^2$ [33]. Another relation related to the result of Eq. (17) can be obtained by integrating $S(\bar{K})-N$ as [27]

$$\begin{aligned}\int_0^\infty d\bar{K}\,\bar{K}^2[S_I(\bar{K})-N]&=\lim_{r_{12}\to 0}[\bar{P}_0(r_{12})/r_{12}^2]\\&\quad-4\pi^2\int d\mathbf{r}\langle\rho(\mathbf{r})^2\rangle_{\mathrm{VT}}\\&=\pi\bar{h}(0)-4\pi^2\int d\mathbf{r}\langle\rho(\mathbf{r})^2\rangle_{\mathrm{VT}}\end{aligned} \tag{18}$$

which can be combined with Eq. (17) to obtain the result for $\bar{h}(0)$ as

$$\bar{h}(0)=[1-2/(\pi\bar{K}_{\max})]^{-1}\left[\frac{1}{\pi}\int_0^{\bar{K}_{\max}}d\bar{K}\,\bar{K}^2[S(\bar{K})-N]+4\pi\int d\mathbf{r}\langle\rho(\mathbf{r})^2\rangle_{\mathrm{VT}}\right] \tag{19}$$

where $\bar{K}_{\max}$ is sufficiently large so that the first term in Eq. (17) provides a valid description of the asymptotic behavior. Equation (19) assumes that one knows the last term on the right from another source. If this last term is insensitive to electron correlation we might expect the approximate equation

$$\Delta\bar{h}(0)\approx[1-2/(\pi\bar{K}_{\max})]^{-1}\left[\frac{1}{\pi}\int_0^{\bar{K}_{\max}}d\bar{K}\,\bar{K}^2\Delta S_I(\bar{K})\right] \tag{20}$$

to hold where the Δ's signify experimental minus Hartree-Fock (HF) molecular quantities. Equations (13) and (17) can be employed to fit the momentum transfer dependence of $S_I(\bar{K})$ to the appropriate power-series expansion in powers of $\bar{K}$ in order to obtain additional correlation-sensitive information.

The integral of the function $S_I(K)-N$ over momentum transfer is also of interest and can be shown to be proportional to potential energy quantities as [13]

$$(2/\pi)\int_0^\infty dK[S_I(K)-N]=V_{ee}-V_{ee}^{\mathrm{cl}} \tag{21}$$

where

$$V_{ee}=\int_0^\infty dr_{12}\bar{P}_0(r_{12})/r_{12} \tag{22}$$

is the electron-electron repulsive potential energy of the molecule and

$$\begin{aligned}V_{ee}^{\mathrm{cl}}&=\int d\mathbf{r}_1\int d\mathbf{r}_2\langle\Psi_V\Psi_T|\rho(\mathbf{r}_1)\rho(\mathbf{r}_2)|\Psi_V\Psi_T\rangle/r_{12}\\&=\int_0^\infty dr_{12}\bar{P}_0^{\mathrm{cl}}(r_{12})/r_{12}\end{aligned} \tag{23}$$

is the classical electron-electron repulsive potential energy between two molecular charge distributions $\rho(\mathbf{r})$. All the foregoing energy quantities are in Rydberg atomic units. While the quantities introduced in Eqs. (13)–(23) are of interest they will yield at most only a few experimental numbers as opposed to a detailed measurement of $S_I(\bar{K})$ which might be characterized by as many independent measurements as time, patience, and angular resolution allow. In this paper 25 new values of $S_I(\bar{K})$ are presented.

An interesting question is, how do we best display the sensitivity of experimental values of $S_I(\bar{K})$? Two unique ways suggest themselves [15,24]. Because the electron-correlation contribution to the total electronic energy of the system is defined as the difference between the nonrelativistic total experimental and Hartree-Fock electronic energies and since $S_I(\bar{K})$ is a linear function of the energy [this can be deduced from Eq. (21) and the virial theorem] we may define the correlation effect on it as

$$[\Delta S_I(\bar{K})]_{\text{corr}}=[S_I(\bar{K})]_{\text{expt}}-[S_I(\bar{K})]_{\text{HF}} \tag{24}$$

where expt stands for the experimentally determined function and HF stands for theoretically calculated values using a Born-Oppenheimer Hartree-Fock molecular wave function with suitable VRT averaging. Now that many HF or near-HF wave functions are available [34,35], Eqs. (11) and (21) should prove to be especially useful for observing the effects of electron correlation in a sensitive manner. A second type of comparison is suggested by the fact that the chemical binding energy is defined by the difference between the total molecular energy and the sum of the atomic energies. For the reasons given above, a comparison function for contributions to $S_I(\bar{K})$ from chemical binding only can be defined as

$$[\Delta S_I(K)]_B=[S_I(\bar{K})]_{\text{expt}}-\sum_{n=1}^{M}[S_n(\bar{K})]_{\text{CI}} \tag{25}$$

where $[S_n(\bar{K})]_{\text{CI}}$ is an accurate description of the x-ray incoherent scattering factor for the nth of M atoms in the molecule. The calculation must be carried out on the ground electronic state of the atom and the result should be averaged over all orientations in space. The subscript CI stands for configuration interaction, which currently may be the best way to obtain the atomic quantities at the accuracy level required ($>95\%$ of the total correlation energy). Unfortunately $S_n(\bar{K})_{\text{CI}}$ values of the required accuracy are not yet available for atoms of primary interest (N, O, or C). Note that by use of Eqs. (21), (24), and (25) contributions to the total electronic correlation energy and binding energy from $[S_I(\bar{K})]_{\text{expt}}$ can be readily estimated as

$$(2/\pi)\int_0^\infty d\bar{K}[\Delta S_I(\bar{K})]_{\text{corr},B}=\Delta V_{ee}(\text{corr},B)-\Delta V_{ee}^{\text{cl}}(\text{corr},B) \tag{26}$$

where $\Delta V_{ee}(\text{corr},B)$ and $\Delta V_{ee}^{\text{cl}}(\text{corr},B)$ are the correlation (corr) or binding (B) contribution to the total electron-electron repulsive potential energy and its classical counterpart, respectively. The use of ΔV above is defined in the same way as for $\Delta S_I(\bar{K})$ in Eq. (24). As an interesting aside, note that the frequently occurring difference, $V_{ee}-V_{ee}^{\text{cl}}$, looks very much like the definition of an exchange or nonclassical (quantum) contribution to the potential energy. Note also that in scattering space $S(\bar{K})-N$ is the variance in the classical electron-electron elastic scattering amplitude.

In summary, we have pointed out a number of useful quantities which should provide rigorous checks on the results of many-body theory. At the same time a number of constraints on the experimental data have been imposed and it is worth keeping these in mind in reading the next section on experimental details. Specifically these are described in (1)–(5) below.

(1) The first Born approximation of scattering theory must provide a valid description of the experiment.

(2) The factorization approximation used to separate exchange from direct scattering must be valid.

(3) The energy resolution of the spectrometer must be sufficient to yield accurate values of the sum rules needed.

(4) The data must be collected at or be correctable to constant momentum transfer $\bar{K}$.

(5) The data must be capable of being accurately extrapolated to infinite energy loss.

In addition to these general constraints a number of technical problems must be considered and it must be kept in mind that any theoretical attempt to produce numbers for comparison with experiment must properly include the effects of VRT motion on the molecule.

III. EXPERIMENT

The experimental setup is depicted in Fig. 1. It consists of two connecting vacuum chambers, the larger of which we denote as the main or scattering chamber and the smaller as the energy analyzer chamber. The scattering chamber is a cylinder of height and radius 60 cm. The circular end of the cylinder is horizontal to the ground plane. A telefocus electron gun [36] is mounted on a turntable inside the chamber and a gas nozzle assembly is mounted on top of it with the effusive gas jet target axis parallel to the vertical cylinder axis. The electron beam current is electronically regulated [37]. The electron beam moves in the horizontal plane and the rotating table on which it is mounted contains a 35-cm-diameter hole in its center so that the gas nozzle has an unobstructed view of the entrance to a cold trap mounted on a 10-in. oil diffusion pump (5300 ℓ/sec pumping speed for air; 2150 ℓ/sec including the baffle). The position of the gas nozzle inlet system can be adjusted from outside the vacuum system to align the target with respect to the axis of rotation of the rotating table and the scattering plane. Target densities have been measured absolutely to an estimated accuracy of 10% [38] although another means of obtaining intensities on an absolute scale is used in this work. The electron gun has electrostatic deflectors which make it possible to place the electron beam in the horizontal plane passing through the center of rotation of the table. A special centering advice, that can be withdrawn from the scattering region and is operated from outside the vacuum chamber, is used to obtain alignment of the gas nozzle when the system is under vacuum. Externally mounted telescopes not shown in Fig. 1 are used for observation during the alignment. In addition, the gas inlet nozzle made of Pt, is electrically isolated from its surroundings and connected to a picoammeter in order to facilitate the alignment process. Further alignment is obtained by measuring the electron current hitting the gas nozzle when it is lowered into the path of the electron beam. Observation of the right-left symmetry of the elastic scattering about the apparent zero scattering angle fixes the final choice of the zero angle.

A Faraday trap is mounted on the turntable for monitoring the unscattered beam during an experiment and can be positioned by use of motors inside the vacuum chamber. There is another Faraday trap located inside an extension (also not shown in Fig. 1) attached to the main chamber at approximately 45° from the energy analyzer direction. At the same distance from the scattering center as the analyzer entrance slits there is, in this Faraday trap arm, a 100-μm acceptance aperture in

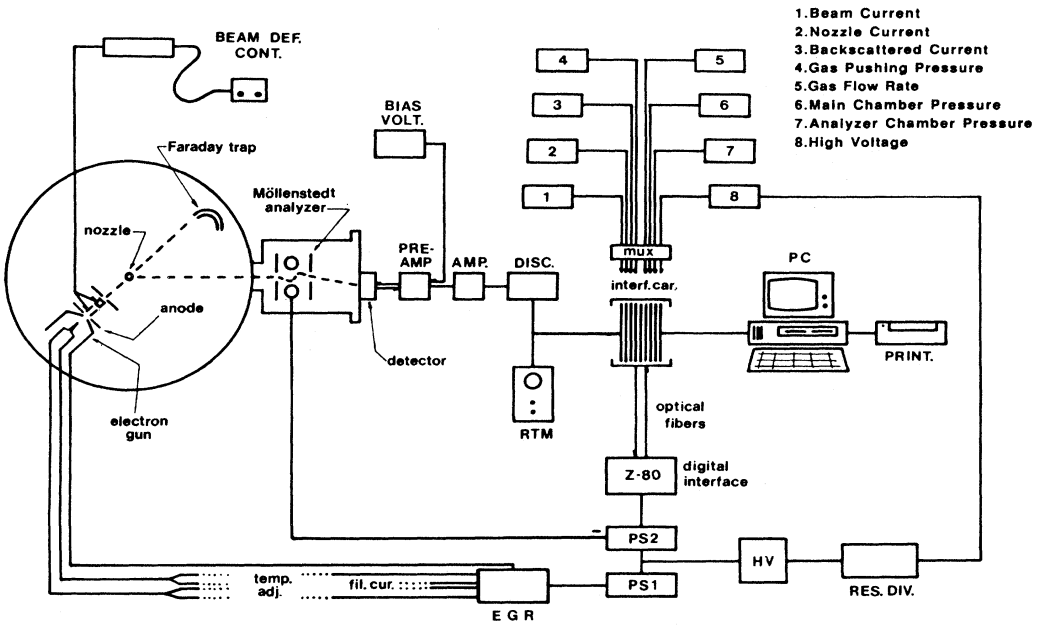

FIG. 1. Schematic diagram of the experiment and its associated data processing electronics. The dotted lines inside the vacuum chambers represent the trajectories of unscattered (into the Faraday trap) and scattered (into the analyzer) electrons. Acronyms defined as BEAM DEF. CONT.: beam deflector controller; E.G.R.: electron gun regulator (temp. adj.: temperature adjustor; fil. cur.: filament current); HV: high-voltage power supply (with bias power supplies PS1 and PS2); RES. DIV.: resistor divider; BIAS VOLT.: detector bias voltage supply; PRE-AMP.: preamplifier; AMP.: amplifier; DISC.: discriminator; RTM: ratemeter; interf. car.: computer interface cards.

front of the trap. This arm aperture is also supposed to be in the horizontal plane that contains the main axis of the collimating slits located at the entrance of the analyzer chamber. By placing the direct beam into this arm it is possible to verify and improve the shape and spatial characteristics of the beam before starting any data collection. The wehnelt cylinder of the electron gun can also be moved from outside the vacuum by use of a motor in order to vary the distance between the inner and outer wehnelt cups which changes the position of the focal point of the electron beam. In front of the electron gun, just after its deflector plates, there is a large circular flat plate which is used to monitor the current of electrons that are scattered back towards the gun.

In operation, the electron beam is focused on the entrance slits of the analyzer which are 99 cm from the scattering center. Two pairs of collimating slits are located just in front of the analyzer chamber entrance slits which are 71 cm from the scattering center. All of these slits may be adjusted from outside the vacuum system and are used to limit the region of the scattering volume viewed by the analyzer in order to eliminate extraneous background and to improve energy resolution. Solid angles of acceptance for the energy analyzer varied from 10^{-5} to 10^{-8} sr depending on the desired energy resolution and count rate. A typical background count rate was less than 1 count/sec.

The analyzer chamber is a cylinder on its side of 30 cm diameter and 75 cm length. The analyzer itself is of the Mollenstedt type and a model similar to the one used here has been described elsewhere [39]. All alignment procedures for the analyzer can be carried out manually from outside the vacuum chamber. The energy-loss spectrum for a fixed scattering angle is scanned electronically. Both chambers are lined inside with magnetic shielding material and the entire apparatus is surrounded by three pairs of Helmholtz coils. The residual field along the entire path of detected electrons is less than 2 mG.

For the work presented here a 25–28-keV incident electron beam with a beam current of 1–50 μA was used to collect relatively complete energy-loss spectra from 0 up to 1000 eV over the scattering angle range of 0.6°–4.2° with an energy resolution of 2–4 eV. The energy resolution was controlled by the Mollenstedt entrance slit setting. Gas flow rates of 13 standard cubic centimeters per minute (SCCM) (10^{18} molecules/sec) resulting in a background scattering chamber pressure of 70–80 μTorr were employed. The energy analyzer chamber was maintained at 4–5 μTorr. Data were collected under computer control. As long as the valence and core spectra were well separated the data collection (offset by -9 V in order to include the whole elastic line) was made in two separate blocks, one for each spectral region. In the first block measurements were made from 0 up to 240 eV and in the second block from 398 to 500 eV in steps of 0.4 and 0.6–0.8 eV, respectively. The number of scattering events at each energy loss were recorded for 1–2 sec in the first block and for 3–10 sec in the second block depending on the angle. At the end of each block 6–10 additional points were measured at selected energy loss

values up to 396 eV in the first block and from 500 to 800–1000 eV in the second block. We shall refer to them as preset count mode points. The density of these sampled points decreased with increasing energy loss in each case. Each of these points was measured with near 3% statistical accuracy. The sparsely spaced end points in the second block were used to extrapolate the GOS to higher energy-loss values. In Fig. 2 a typical spectral scan is displayed. As the scattering angle was increased, the point in the valence block at which the mode for data collection changes was also increased. At this point, located on the high-energy loss side of the Bethe ridge, the intensity was near 20% of the valence-shell maximum.

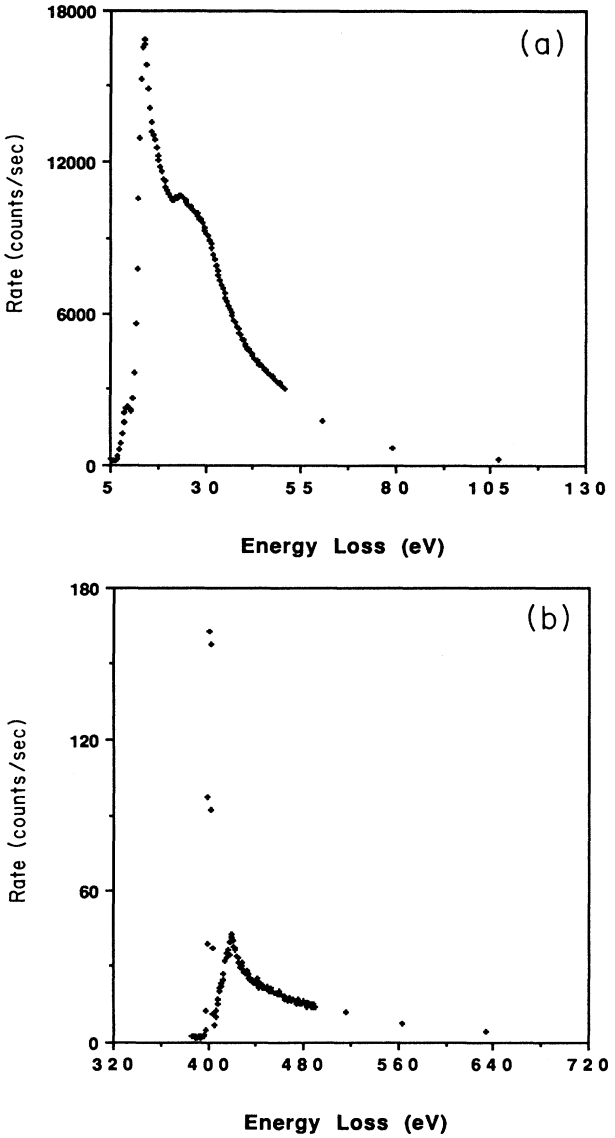

FIG. 2. A typical spectrum for N_2 at $\theta \simeq 0.8°$. The upper figure shows the valence-shell data block and the lower figure shows the core spectrum. Note that the sparsely spaced points at the high-energy-loss end of each figure are points obtained with 3% statistical accuracy.

In this experiment, detection of scattered electrons was made with a silicon surface barrier detector. A dead-time correction was experimentally determined and was routinely used to correct the collected experimental intensities $I^{\rm col}_{\rm expt}(\theta,E)$ as

$$I_{\rm expt}(\theta,E)=I^{\rm col}_{\rm expt}(\theta,E)[1+\tau I^{\rm col}_{\rm expt}(\theta,E)] \ . \tag{27}$$

The dead time τ was obtained from a plot of the ratio $R=I^{\rm col,inel}_{\rm expt}/I^{\rm col,el}_{\rm expt}$ versus $\Delta I=I^{\rm col,el}_{\rm expt}-I^{\rm col,inel}_{\rm expt}$ where $I^{\rm col,el}_{\rm expt}$ refers to the maximum number of counts/sec for the elastic line and $I^{\rm col,inel}_{\rm expt}$ is the corresponding quantity for the first prominent inelastic feature observed. Since

$$\epsilon+\epsilon\tau\Delta I=R \ , \tag{28}$$

where $\epsilon=I^{\rm inel}_{\rm expt}/I^{\rm el}_{\rm expt}$ is the true ratio between intensities which must be a constant independent of the count rate, the slope of such a plot is $\epsilon\tau$ with ϵ being the intercept. A linear fit of 30 points of R and ΔI values, obtained at incident beam currents from 1.5 up to 60 μA, yielded a dead-time correction for the detector employed in this experiment of $\tau=(3.04\pm0.03)\times10^{-6}$ sec. Collection of R and ΔI values was made at a fixed angle of 0.8°.

After the relative experimental intensities $I_{\rm expt}(\theta,E)$ were obtained they were converted to a relative GOS by use of the formula [40]

$$\left[\frac{df(K(E),E)}{dE}\right]_{\rm rel}=I_{\rm kin}(\theta,E) \times[I_{\rm expt}(\theta,E)-B(\theta,E)] \times K_{\rm Kol}(E)/F_{\rm ex}(\theta,E) \tag{29}$$

where

$$I_{\rm kin}=\frac{E(1-\beta^2)k_i[K(E)^2-E^2/4c^2]^2}{4k_f(E)K(E)^2[1-(E/2c^2)^2(1-\beta^2)^{1/2}]} \ ,$$

$$K_{\rm Kol}(E)=[E_0/(E_0-E)]^a \ ,$$

$$F_{\rm ex}(\theta,E)=1-[K(E)/k_f(E)]^2+[K(E)/k_f(E)]^4 \ ,$$

$$k_i^2=E_0(1+E_0/4c^2) \ ,$$

$$k_f^2(E)=k_i^2-E[1+(E_0/2c^2)-(E/4c^2)] \ ,$$

and

$$K(E)^2=k_i^2+k_f^2(E)-2k_ik_f(E)\cos\theta \ .$$

In Eq. (29), $I_{\rm kin}$ is a kinematic factor which includes relativistic corrections for the incident electron of energy E_0; β is the ratio of the velocity of the incoming electron to the velocity of light c; θ is the scattering angle; $F_{\rm ex}$ is a correction for exchange scattering assuming the validity of the factorization approximation (this is just the ratio of the Mott to Rutherford cross sections for electron-electron scattering); and the expressions for k_i, $k_f(E)$, and $K(E)$ are relativistic. $B(\theta,E)$ is a background correction. Measurements which reproduced the 70–80-μTorr background pressure by moving the nozzle 1–2 cm out of the scattering center were carried out. In order to avoid the time consuming collection of background

data points for each spectral scan, the background was carefully checked only at a few selected angles ($-1.55°$, $+1.6°$, and $+2.35°$). At these angles the deviations in $\Delta S_I(\bar{K})$ were less than 4%. It was assumed that $B(\theta,E)$ does not make an important error and no attempt was made to correct for it in this work for other scattering angles. This does not mean that there are no significant background errors. It only means that the background scattering that we are able to artificially produce is small and has roughly the same shape as the experimental GOS itself. In fact we discovered that assuming the existence of a straight line background with zero or negative nonzero slope yielded a progressively serious correction with increasing K. It is bothersome to note that the count rate at $E=-9$ eV is actually greater than the signal observed at 1000 eV. Whether this is due to scattering off the beam trap or from backscattering from the electron gun which only takes place when the gas jet is in its experimental location, and hence is localized to the immediate vicinity of the elastic line, is not known. What we can say is that the addition of a straight line background causes an increasing correction to $\Delta S_I(\bar{K})$ with increasing $\bar{K}$ which reduces its values [makes $\Delta S_I(\bar{K})$ less negative]. In other words, since $\Delta S_I(\bar{K})$ is sensitive to such a background for $\bar{K}>1.6$ a.u., our results represent an upper bound within the uncertainty from other error sources to be discussed later.

In Eq. (29), K_{Kol} is the Kollath correction [41] which corrects the intensity for the fact that the analyzer energy resolution increases with decreasing kinetic energy of the detected electron. The exponent value a in the K_{Kol} expression was experimentally determined for the Mollenstedt analyzer used in this work by measuring the spread of the elastic line (ΔE) at different energies E over the range from $E_0=25$ down to 24 keV. The exponent value, $a=0.53\pm0.05$, was the slope in the $\log\Delta E$ versus $\log(E_0-E)$ curve and it does not agree with the value proposed in Ref. [41] ($=0.67$) due to differences between the analyzers.

Once the relative GOS was determined the GOS corresponding to the preset count points of the core spectra were least-squares fitted with theoretical data generated from the formula [42]

$$\frac{df(K,E)}{dE}=[N_t E(E-I)^{1/2}\lambda^3 P]\{\lambda^2[4(K+q_c)^2-(q_c^2+\lambda^2)]-6\lambda^2 q_c(K+q_c)+\lambda^2(3q_c^2+\lambda^2)\}/[3\pi K^6(q_c^2+\lambda^2)^3] \tag{30}$$

where

$$q_c=(E-K^2-I+\lambda^2)/2K\ ,$$

$$P=\{2\pi\gamma/[1-\exp(-2\pi\gamma)]\}\times\exp\{-2\gamma\arctan[\lambda(E-I)^{1/2}/(\lambda^2-Kq_c)]\}\ ,$$

and

$$\gamma=\lambda/(E-I)^{1/2}$$

with I the ionization potential of the tail electrons, and N_t and λ being the number of electrons contributing to the tail and the effective charge of the ion observed by the ejected electron, respectively. We shall refer to Eq. (30) as the hydrogenic tail. In this work, N_t and λ were adjusted to give the best least-squares fit to the experimental preset count points with I fixed at the experimental value for the most tightly bound orbital of the core.

The use of Eq. (30) as a model for the missing tail requires justification. To do this we fitted numerical data [43] for the optical oscillator strength for atomic nitrogen from 600 to 1000 eV and discovered that the hydrogenic model was capable of predicting the results above 1000 eV up to 14 000 eV with three-significant-figure accuracy. This provides a valid test for N_2 at small momentum transfers since it has been shown that the molecular oscillator strength is virtually identical to twice the atomic value at these energies [44]. Unfortunately, atomic and molecular GOS ($K\neq0$) theoretical values do not yet exist for nitrogen. Equation (30) was therefore checked against theoretical GOS values for atomic hydrogen [43] over a wide range of $\bar{K}$ values to make sure that the equation was correctly programmed.

Once Eq. (30) was least-squares fitted to the experiment using the experimental $K(E)$ values it was then used to calculate the missing tail area which was estimated by numerical integration. In addition, the function AE^{-b} was least-squares fitted to the same experimental data and the value of A and b obtained were used to calculate the missing area by analytical integration. This function provided an upper bound on the missing area. A lower bound was established by fitting the function $AE^{-3.5}$ to the last experimental point in the GOS and integrating it analytically to obtain the missing area. The integration procedures were checked by use of the theoretical data for atomic nitrogen where the missing area has been accurately determined. It was found that the hydrogenic tail model gave excellent agreement with the known value and was about one-fourth of the difference between the two bounds from the AE^{-b} function result. This ratio was roughly found to be the case for the data at different K values. Hence we conclude that the hydrogenic model is the best vehicle we have at present for estimating the missing area. A subtle point is that of the three models only the hydrogenic model can furnish an estimate of the missing area for $\bar{K}$ as opposed to $K(E)$. Although both the $AE^{-3.5}$ and the hydrogenic models have the correct asymptotic dependence on E [45] this does not seem to be an important criteria as witnessed by the fact that the hydrogenic model gives an area much closer to that of the AE^{-b} model where b is typically found to be around 2.5.

After getting GOS values by means of Eqs. (29), for the collected points, and (30), for the missing tails, they were then placed on what can be called a near-absolute scale which will be justified as follows. Since at this point GOS values with respect to constant momentum transfer $\bar{K}$ were still not available, the use of the Bethe sum rule $S(0,\bar{K})=N$ should not be, at least theoretically, em-

ployed yet. Figure 3 shows how $K(E)$ values deviate from $\bar{K}$ values defined by the binary encounter approximation as [13]

$$\bar{K}^2 = E_0 \sin^2\theta \ . \tag{31}$$

Because $K(E)$ should be close to $\bar{K}$ for small E values ($E < 300$ eV) we performed a first normalization of our relative GOS distribution by use of the Bethe sum rule using only the valence-shell block data with an added AE^{-b} tail. A sum rule value of 10 was employed which assumes that variation from 10 due to the omission of excitations to the $1s\sigma$ states is not strongly K dependent.

The next step involved correcting the data from constant angle to constant momentum transfer which was accomplished by use of the truncated McLaurin series expansion [46]

$$\frac{df(K(E),E)}{dE} = \frac{df(\bar{K},E)}{dE} + [K(E)^2 - \bar{K}^2]\left[\frac{d}{dK^2}\right]\frac{df(K,E)}{dE} \tag{32}$$

where the derivative is evaluated at $K(E)$ and $\bar{K}^2$ is the binary encounter value given by Eq. (31) which greatly simplifies the expressions for the corrections. This choice also means that the average energy loss is given as $\bar{E} = E_0 \sin^2\theta$. If $K^2(E)$ is expanded in a McLaurin series about $\bar{E}$ and the approximate result

$$K(E)^2 - \bar{K}^2 = (E - E_0 \sin^2\theta)^2 / 4E_0 \tag{33}$$

is inserted into Eq. (32) and used to evaluate the various sum rules by interchanging the order of carrying out the sum and the differentiation with respect to K^2, we obtain

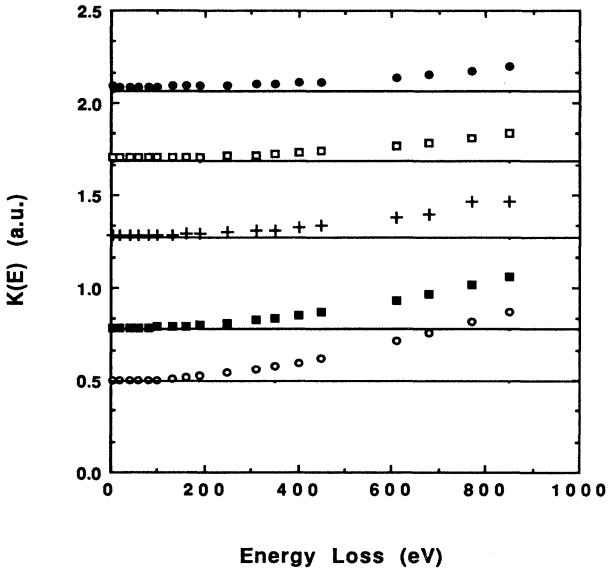

FIG. 3. The variation of $K(E)$ with energy loss at fixed scattering angles: ○, 0.6°; ■, 1.0°; +, 1.6°; □, 2.1°; ●, 2.5°. The difference between the horizontal solid line and the points in each case constitute the correction $[\bar{K} - K(E)]$.

$$S_p(l,E_0,\theta) = S_p(l,\bar{K}) + \left[\left[\frac{d}{dK^2}\right]S_p(l+2,K) - 2\bar{E}\left[\frac{d}{dK^2}\right]S_p(l+1,K) + \bar{E}^2\left[\frac{d}{dK^2}\right]S_p(l,K)\right] \Big/ 4E_0 \tag{34}$$

where the subscript p on the sums indicates that they are carried out only over the experimental data range. Equation (34) was used to correct the sums from constant θ values to constant K values. It is assumed that the derivatives at constant $K,\bar{K}$, are approximately the same as those at constant angle. This assumption was partially justified by the smallness of the resulting corrections. Plots of $S_p(l,\bar{K})$ versus $\bar{K}^2$ for $l=2$, 1, 0, and -1 are shown in Fig. 4. Polynomials in $\bar{K}^2$ were least-squares fitted to those curves and the required slopes obtained from the fit by analytic differentiation. Missing tail areas were added to the resultant constant K corrected values of the $S_p(l,\bar{K})$'s by use of the hydrogenic tail given by Eq. (30) for each value of $\bar{K}$. The sums of interest, $S(0,\bar{K})$ and $S(-1,\bar{K})$, were then renormalized by use of the Bethe sum rule with respect to $N=14$.

The assumption of approximating constant K slopes by use of slopes at constant θ is justified by the fact that the largest corrections are of the order of 1%. In general, the largest corrections are to the Bethe sum rule increasing its value. This has the effect of decreasing the value of $S_I(\bar{K})$ and hence increasing the effect of correlation. As a final check on our correction procedure we used Eq. (32) in the same way as Eq. (34) to estimate the constant angle to constant K correction at 850 eV energy loss and compared this with the prediction of the hydrogenic tail model. The corrections were found to be small. For instance, the corrections $[df(\bar{K},E)/dE - df(K(E),E)/dE]$ for the smallest and largest angles were -0.0046 and -0.0061, respectively, compared to $-0.000\,87$ and 0.0012 predicted by the hydrogenic model and amounted to 4% and 2.5% of $df(\bar{K},E)/dE$.

Once the sums are corrected to constant K a correction for the effect of energy resolution is applied as [47]

$$S_I(-1,\bar{K}) = S_I(-1,\bar{K})_{\text{expt}} - \langle x^2\rangle S_I(-3,\bar{K})_{\text{expt}} - \langle x^3\rangle S_I(-4,\bar{K})_{\text{expt}} \tag{35}$$

where the $\langle x^n\rangle$ are energy moments of the spectrometer resolution function which we calculate from the elastic line intensity $I(E)_{\text{el}}$, since our resolution is always significantly larger than the natural linewidth, as

$$\langle x^n\rangle = \int dE(E-E_0)^n I(E)_{\text{el}} \Big/ \int dE\, I(E)_{\text{el}} \tag{36}$$

with the integrations carried out over the width of the elastic line. Note that the zero of the energy loss scale is given by

$$E_0 = \int dE\, EI(E)_{\rm el} \Big/ \int dE\, I(E)_{\rm el} \qquad (37)$$

and that the constant angle to constant K correction is made before the energy resolution correction. This correction is less than 0.5% in all cases studied and vanishes for the $S(0,\bar{K})$ sum.

IV. ERROR ANALYSIS

The errors can be classed as those contributing to the scattering angle, energy loss, intensity (GOS), and the sum rules. The errors contributing to the determination of the scattering angle are the linearity and accuracy of the angle scale, determination of the zero angle, and magnetic field distortions. The angle was determined by reading a steel rule fastened to the circumference of the turntable on which the electron gun was mounted. The rule was obtained from the Bridgeport Milling Machine Co. and was ruled in 0.1 mm divisions and was read through a window in the vacuum chamber wall by means of a microscope. The turntable radius was machined so that 1 cm along the circumference corresponded to 1°. The scale was calibrated by use of a theodolite and the relative angular accuracy and linearity were established to be better than ±0.001° over the range of scattering angles ±20°. As mentioned previously the magnetic field was reduced below 2 mG so that no correction for magnetic distortion was found to be necessary. The absolute angle scale was established by making measurements of the

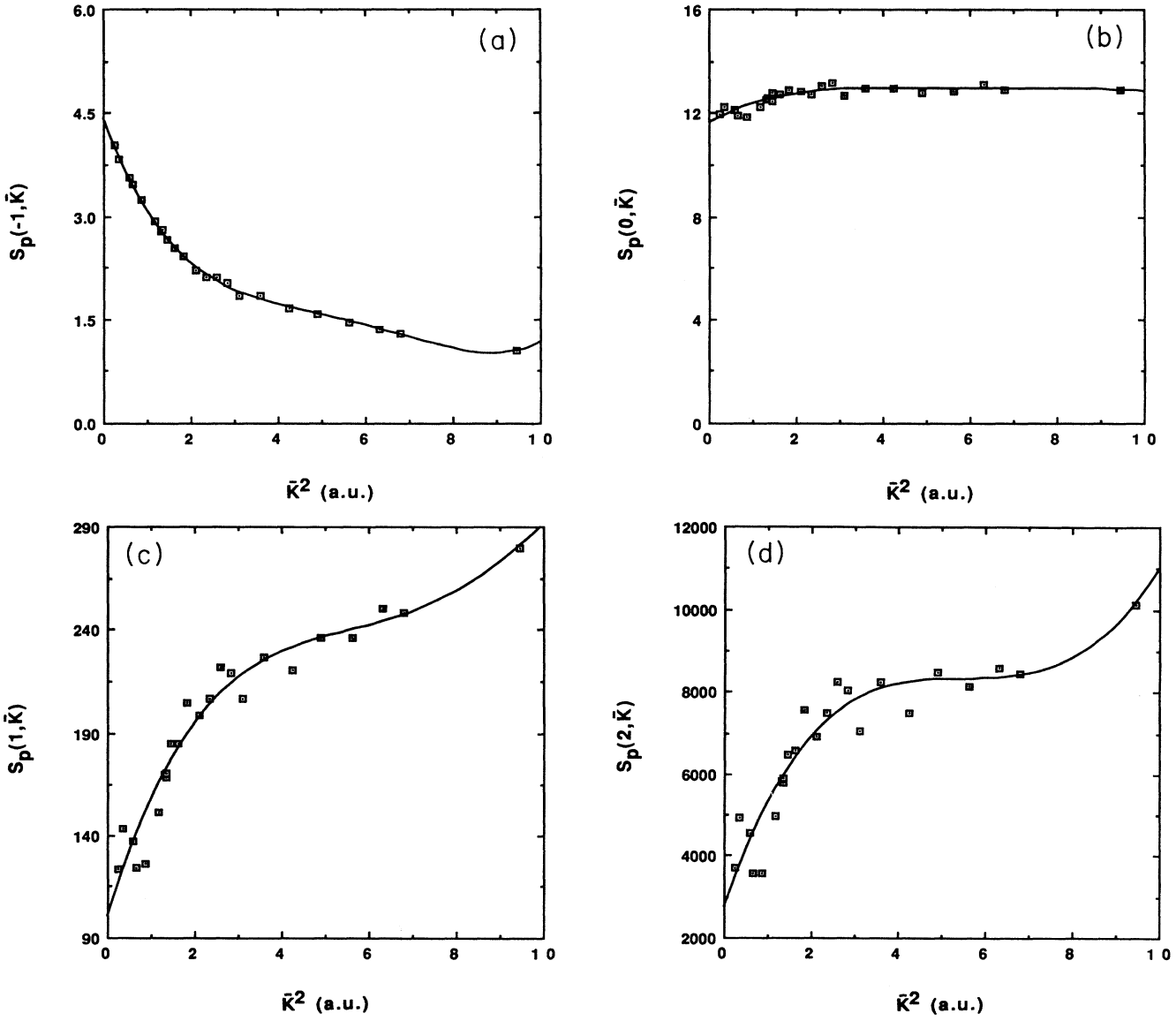

FIG. 4. The variation of $S_p(-1,\bar{K})$ (a), $S_p(0,\bar{K})$ (b), $S_p(1,\bar{K})$ (c), and $S_p(2,\bar{K})$ (d) with $\bar{K}^2$ for the data sets used in this study.

elastic line intensity at both positive and negative scattering angles and adjusting the choice of the zero angle until the sum of the squares of the differences between the two sides was minimized. Data points on one side were obtained at the same angles as the other side by interpolation. The uncertainty of the zero-angle determination was estimated to be less than 0.005° so that the overall error estimate for the scattering angle was taken as ±0.005°.

The energy-loss scale was calibrated by offsetting the elastic line by use of a calibrated floating power supply biased to the power supply furnishing the accelerating potential for the electron gun. This was done in steps of 100 V over the range from zero to 1000 V. The centers of gravity of the lines were then determined and the apparent positions in channel numbers were least-squares fitted to the actual voltages using a cubic polynomial. These fits were linear to about one part in 10^6 and established the linearity of the energy-loss scale. The absolute energy-loss scale was then determined from the center of gravity of the elastic line for each spectral scan. The resolution of the digital-to-analog converter used to scan the energy-loss scale was 45 mV with an uncertainty on the order of 15 μV since we used a 16-bit converter. Considering that the load regulation accuracy of the floating power supply was 0.01% as specified by the manufacturer we decided to take 0.03% as the estimate of the energy-loss uncertainty.

Because the determination of $S_I(\bar{K})$ involves multiplying the intensity by $\bar{K}^4$ it is important to consider the error in the determination of K. In addition to the scattering angle and energy loss the error in determining the incident energy must also be considered. The accelerating voltage was monitored by use of a commercial resistance divider (model HVP-250; Computer Power System, Inc.) calibrated by the manufacturer to 0.03% at 30 kV. Two of these dividers were purchased and are periodically compared to make sure that the calibration has not changed. We have taken the uncertainty in the accelerating potential to be ±10 V. Using the above uncertainties and the ranges of E and θ used in the experiment along with an incident energy of 25–28 keV we find that the main contribution to the error in K comes from the angular uncertainty. The simple formula $\Delta K^2 = 2E_0\theta\Delta\theta$ yields an excellent estimate of the error in K^2.

The errors affecting the GOS are the statistical error from the total number of events recorded, the variation of detector efficiency with electron-impact energy, failure of the Born approximation, failure of the factorization approximation, the Kollath correction, dead-time corrections, multiple scattering corrections, and density variations in the scattering volume as viewed by a finite detector solid angle.

The intensities are measured by repeated scans of the entire energy-loss spectrum which requires from a few minutes to several hours per scan depending on the scattering angle. Each scan is saved in the computer and the spectrum for each scattering angle consists of the average of at least six scans. The average scan is then compared with each individual scan to make sure that the repeatability of the experiment is within the statistical uncertainty as determined from the total number of counts. The statistical uncertainty of the GOS is better than 1% near its maximum but since the total number of counts in a sum rule is extremely large one might assume the statistical errors in sum rules to be negligible. This is certainly true for the $S(-1,K)$ sum rule since for constant K it is essentially a straight sum over the intensities and hence its statistical error is proportional to the square root of the sum of all counts accumulated in the sum. Timing uncertainty is assumed to be 1 part in 10^4 since a 10-kHz clock was used for data collection under computer control. The error in the Bethe sum rule is complicated by the fact that the intensities are multiplied by the energy loss and the error in the energy-loss scale becomes a factor. A simple model with the correct asymptotic energy-loss behavior suggests that the dominant error comes from the term proportional to the error in the energy loss.

Detector efficiency changes were shown to be negligible by comparing the total number of counts in the elastic line at a fixed scattering angle, normalized by dividing by the incident electron beam current and corrected for the energy dependence of the elastic cross section [48], for incident electron beams of 28- and 27-keV energies. It is well known that corrections for backscattering of electrons by Si are extremely constant over a wide range of impact energies [49]. This error source will be ignored. Note that the constant detection efficiency over a very large energy-loss range is what gives the electron-scattering method an important advantage over photoabsorption spectroscopy.

The validity of the Born approximation has been tested extensively in this energy range by others [14,50] and found to be valid within the experimental accuracy by comparing GOS values obtained at different energies as a function of K. This test also confirms the validity of the factorization approximation since the exchange scattering depends strongly on E_0 as well as K. Note that the ratio of the Mott to Rutherford cross sections at the energies and angles used in this study deviates from unity by at most 0.5%.

The Kollath correction was discussed in a preceding section of this paper and is routinely made to the data, with a maximum 6% correction occurring at the largest energy-loss value. Error caused by this procedure to the collected intensities is negligible. Details of its contribution to the counting errors will be shown in the error model to be described.

Error from the possibility of intermolecular multiple scattering has been considered elsewhere for experiments of this type and incident energy [51] with the conclusion that, using the experimental conditions employed in this study, no multiple scattering should contribute within the accuracy of the experiment.

Dead-time corrections were also routinely made although since all inelastic count rates were less than 10 kHz the magnitude of this correction never exceeded 4%. Errors in the intensity caused by the detector opening angle and density variations in the scattering volume are also negligible for the experiments reported here [52].

In analyzing the errors in $S_I(\bar{K})$ obtained by use of the

sum rules we will neglect errors in all the small corrections that are routinely made as discussed above. In addition, the error in the numerical integration schemes used to obtain the sum-rule sums were estimated by applying them to the integration of a Gaussian peak of 2-eV full width at half maximum (FWHM) with an energy-loss spacing of 0.6 eV. The error obtained using a Newton's rule integration scheme was found to be negligible. The error in K^2, the statistical counting errors, the errors in estimating the tail correction with the hydrogenic model, and errors in determining scale factors are treated as follows.

We adopt a simplified version of the relative GOS for the purpose of error estimation which allows us to write the $S(0,K)$ and $S(-1,K)$ sum rules, respectively, as

$$S(0,K)=\alpha(K^2I_0+\beta T_0)=N \tag{38}$$

and

$$S(-1,K)=\alpha(K^2I_-+\beta T_-)=S(K)/K^2 \tag{39}$$

where

$$I_0=\sum_{i=1}^{N} E_iF_iN_i\Delta E \ ,$$

$$I_-=\sum_{j=1}^{N} F_jN_j\Delta E \ ,$$

$$T_0=\sum_{p=1}^{M}\left[\frac{df}{dE}\right]_p\Delta E' \ ,$$

and

$$T_-=\sum_{q=1}^{M}\left[\left[\frac{df}{dE}\right]_q\Big/E_q\right]\Delta E'$$

with the i,j sums being carried out over experimental data points while the p,q sums involve estimated (df/dE) hydrogenic tail values. In these equations N_i is the number of counts per second in the ith channel, E_i is the energy loss for the ith channel, F_i is the associated kinematic factor $I_{\rm kin}$ in Eq. (29) divided by EK^2, ΔE is the energy spacing between collected points, β is the linear normalizing constant factor that matches the theoretical hydrogenic tail to the relative experimental values in the preset count mode region, α is the normalizing constant which places the relative GOS on an absolute scale by use of the Bethe sum rule, N is the number of electrons in the target molecule, and K^2 is the square of the momentum transfer. It is necessary to define the energy loss in terms of channel numbers as

$$E_j=\rho(n_j-\bar{n})$$

where ρ is the scale factor which converts channel number to energy, n_j is the number of the jth channel, and $\bar{n}$ is the channel number of the center of the elastic line which is not necessarily an integer. We will also write the associated kinematic factor as

$$F_j=[E_0/(E_0-E)]^aG_j=L_jG_j$$

where L_j is the Kollath correction as in Eq. (29) and G_j is everything else. We will assume that G_j is without error and consider only the error involved in the experimental determination of the Kollath correction. By assuming that all errors act independently we can write the errors in $S(K)$ as

$$\Delta S(K)=\left[\left[\frac{\partial S}{\partial K^2}\right]^2(\Delta K^2)^2+\left[\frac{\partial S}{\partial\beta}\right]^2\Delta\beta^2+\left[\frac{\partial S}{\partial I_0}\right]^2\Delta I_0^2+\left[\frac{\partial S}{\partial I_-}\right]^2\Delta I_-^2+\left[\frac{\partial S}{\partial T_0}\right]^2\Delta T_0^2+\left[\frac{\partial S}{\partial T_-}\right]^2\Delta T_-^2\right]^{1/2} . \tag{40}$$

After deriving the expressions for the partial derivatives we arrive at the intermediate result

$$\Delta S(K)/S(K)=\{(\Delta K^2/K^2)^2[1+(\beta/K^2)(T_0/I_0-T_-/I_-)]^2+(\Delta I_0/I_{0-})^2+(\Delta I_-/I_-)^2+(\Delta\beta/\beta)[(\beta/K^2)(T_0/I_0-T_-/I_-)]^2+(\Delta T_0/T_0)^2(\beta T_0/K^2I_0)^2+(\Delta T_-/T_-)^2(\beta T_-/K^2I_-)^2\}^{1/2} , \tag{41}$$

where $\beta T_{0,-}$ has been neglected in comparison to $K^2I_{0,-}$.

We have used Eq. (41) to estimate the uncertainties in $S(K)$ by expanding each individual error term, where applicable, in terms of the uncertainties upon which it depends. With the exception of β all other quantities depend upon two or more other variables. The approximate results are

$$(\Delta K^2/K^2)^2=4(\Delta\theta/\sin\theta)^2+(\Delta E_0/E_0)^2+(\theta^2/2)^2\{(\Delta\rho/\rho)^2+[\Delta\bar{n}/(n-\bar{n})^2]\} , \tag{42}$$

$$(\Delta I_0/I_0)^2=(\Delta\rho/\rho)^2+\rho^2(I_-/I_0)^2\Delta\bar{n}^2+\theta^4(\Delta a)^2+\sum_{j=1}^{N}(E_jF_j\Delta E)N_j/I_0^2 , \tag{43}$$

and

$$(\Delta I_-/I_-)^2=\theta^4(\Delta a)^2+\sum_{j=1}^{M}(F_j\Delta E)^2N_j/I_-^2 \tag{44}$$

with a being the exponent used in the Kollath correction in Eq. (29). The remaining two terms can be written as

$$(\Delta T_0/T_0)^2=(1/T_0^2)\left[\left[\frac{\partial T_0}{\partial\lambda}\right]^2\Delta\lambda^2\right] \tag{45}$$

TABLE I. A summary of major sources of uncertainty in the x-ray incoherent scattering factor.

Source	Estimated uncertainty
Scattering angle, θ	$\pm 0.005°$
Energy-loss scale, E	$\pm 0.03\%$ of E
Incident energy, E_0	± 10 eV
Timing uncertainty	1×10^{-4} sec
Channel number—energy-loss conversion factor	0.1%
Kollath correction exponent	10%
$\Delta K^2/K^2$ (momentum transfer)	$<1.8\%$
$\Delta\beta/\beta$ (scaling factor)	$<3\%$
Data collection uncertainty:	
$\Delta I_0/I_0$ [for $S(0,K)$ sum rule]	$<4\%$ for $\theta<1.8°$ $>5\%$ for $\theta>1.8°$
$\Delta I_-/I_-$ [for $S(-1,K)$ sum rule]	$<2\%$ (2.7% at $\theta\simeq 4.1°$)
Hydrogenic tail estimation:	
$\Delta T_0/T_0$ [for $S(0,K)$ sum rule]	$<0.05\%$
$\Delta T_-/T_-$ [for $S(-1,K)$ sum rule]	$<1.5\%$
Overall error	3–6 % (11% at $\theta\simeq 4°$)

and

$$(\Delta T_-/T_-)^2=(1/T_-^2)\left[\left[\frac{\partial T_-}{\partial\lambda}\right]^2\Delta\lambda^2\right] \tag{46}$$

where the partial derivatives of the hydrogenic GOS are evaluated numerically. In the tail corrections we have assumed that there is no error in the energy scale and that errors all come from the least-squares fit to the preset count points. Note that the error in β accounts for the scale match to the data assuming the data are errorless. We have decided to define

$$(\Delta\beta/\beta)^2=(\Delta\beta/\beta)^2+(1/N_{\rm av}) \tag{47}$$

where $(\Delta\beta/\beta)$ on the right of the equal sign is the error estimate of β from the least-squares fit and $N_{\rm av}$ is the total number of counts in the preset count mode which is an estimate of the accuracy of the points being fitted.

A summary of major sources of uncertainty in the x-ray incoherent scattering factor is displayed in Table I. Error bars shown in the figures are based on these errors.

V. RESULTS

Some intermediate $S_I(l,\bar{K})$ sum-rule results obtained in the calculation of $S_I(\bar{K})$ are displayed in Table II. These results serve as checks on the quality and consistency of the data. In this table, the results for the $l=-1$, -2, and -3 sum rules obtained through this work are compared with earlier measurements from our laboratory by Ketkar and Bonham [15]. New values for the sum rules are reported, extending the squared momentum transfer range from 2.3 a.u. (the upper limit in the paper by Ketkar and Bonham) to near 9.5 a.u. For $\bar{K}^2>5.6$ a.u., limiting values for $S_I(l,\bar{K})=N\bar{K}^{2l}$ as $\bar{K}\to\infty$ [20] are also tabulated. The $\bar{K}^2$ range covered in this work was not enough for the experimental values of $S_I(-1,\bar{K})$ to approach the asymptotic limiting values. This does not seem to be the case for $S_I(-2,\bar{K})$ considering the proximity between the last asymptotic and experimental values. For $S_I(-3,\bar{K})$, NK^{-6} calculated values shown in Table II are considerably below the corresponding sum-rule reported values. In Table III, our extrapolated optical values are compared with other results [15,51–53] and are found to be in good agreement. Particularly, $S_I(-2,0)=\alpha_m/4$ with α_m the static molecular polarizability of the target.

In Fig. 5, our experimental values of $S_I(\bar{K})$ are compared with the near-Hartree-Fock values of Epstein and Stewart [34]. The difference function, $[\Delta S_I(\bar{K})]_{\rm corr}$, based on these HF values as a function of $\bar{K}$ is also in-

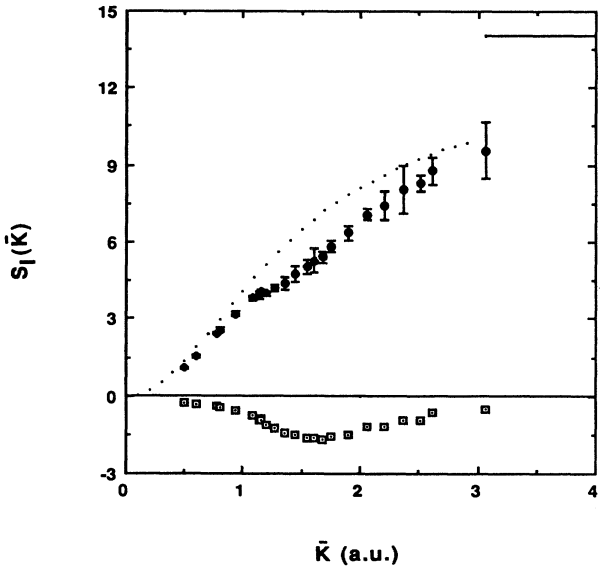

FIG. 5. The Hartree-Fock values of $[S_I(\bar{K})]_{\rm HF}$, $\cdots$; the experimental values of $[S_I(\bar{K})]_{\rm expt}$, ●●●; and the difference $\Delta S_I(\bar{K})=[S_I(\bar{K})]_{\rm expt}-[S_I(\bar{K})]_{\rm HF}$ as a function of $\bar{K}$, ⊡⊡⊡. The horizontal line in the upper right hand corner marks the asymptotic value in the limit as $\bar{K}\to\infty$ (14).

cluded in Fig. 5 to show how intense the electron-correlation effects are on the x-ray incoherent scattering factor. The asymptotic value for this factor as $\bar{K} \to \infty$ [$S(K)=14$, in the case of N_2] is shown in the upper right-hand corner. In Fig. 6, the results for $[\Delta S_I(\bar{K})]_{\text{corr}}$ are magnified and compared with the theoretical results of Breitenstein, Mayer, and Schweig [35] and the experimental data of Ketkar and Bonham [15] and Zhang, Ross, and Fink [56]. The solid curve results are based on a wave function yielding 50–55 % of the valence-shell electron-correlation contribution to the total energy. Vibrational averaging is not included since it is not believed to cause a serious problem [57]. The dotted curve in Fig. 6 represents a scaled set of theoretical values published by Breitenstein, Mayer, and Schweig [35] which would give the correct total correlation energy by assuming that the missing contribution to this total would depend on the momentum transfer in the same way as the calculated values do. Our new results are in agreement with the earlier measurements from our laboratory by Ketkar and Bonham [15] at small $\bar{K}$ but are higher at larger $\bar{K}$ mainly due to improved data correction procedures and to the discovery that the Kollath correction had been inverted in the data analysis program. Our results clearly show that the extrapolated results of Breitenstein, Mayer, and Schweig [35] are incorrect below $\bar{K}=1.3$ a.u. Above 1.3 a.u. the extrapolated results are within our error bars. The experimental results reported by Zhang, Ross, and Fink [56] were obtained by subtracting measured elastic scattering data [56] from total cross-section measurements carried out by Fink and Schmiedekamp [19]. It is worth mentioning that the correlation effect on the elastic scattering for N_2 determined by these authors was considerably larger than the theoretical results available at the time by Breitenstein, Mayer, and Schweig [35] and by Liu, Lie, and Liu [58] which took into consideration 61%

TABLE II. $S_I(l,\bar{K})$ sum rules for N_2 ($l=-1,-2,-3$).

	$S_I(-1,\bar{K})$		$S_I(-2,\bar{K})$		$S_I(-3,\bar{K})$	
$\bar{K}^2$ (a.u.)	This work[a]	Ref. [15][b]	This work[a]	Ref. [15][b]	This work[a]	Ref. [15][b]
0.086		4.72		2.84		2.09
0.114		4.76		2.82		2.08
0.171		4.75		2.76		1.97
0.231		4.64		2.67		1.88
0.241	4.47		2.26		1.62	
0.356	4.28		2.06		1.45	
0.4		4.32		2.31		1.62
0.599	4.03		1.78		1.20	
0.649		3.79		1.81		1.21
0.654	3.89		1.69		1.13	
0.867	3.65		1.48		0.955	
1.0		3.52		1.53		0.882
1.177	3.24		1.19		0.705	
1.294		3.21		1.28		0.760
1.311	3.00		1.11		0.663	
1.346	3.01		1.12		0.679	
	2.98		1.11		0.669	
1.433	2.79		1.01		0.592	
1.435	2.79		1.00		0.587	
1.605	2.61		0.919		0.527	
1.833	2.40		0.850		0.481	
2.088	2.28		0.698		0.363	
2.286		2.62		0.82		0.40
2.340	2.11	2.63	0.653	0.84	0.349	0.42
2.592	2.03		0.654		0.344	
2.822	1.92		0.582		0.294	
3.094	1.89		0.495		0.241	
3.600	1.76		0.490		0.235	
4.252	1.66		0.391		0.176	
4.884	1.52		0.377		0.174	
5.626	1.43	(2.49)[c]	0.308	(0.442)[c]	0.135	(0.0786)[c]
6.320	1.31	(2.22)	0.265	(0.351)	0.113	(0.0555)
6.791	1.29	(2.06)	0.250	(0.304)	0.106	(0.0447)
9.437	1.01	(1.48)	0.167	(0.157)	0.0688	(0.0167)

[a]Error estimates (averaged over $\bar{K}^2$ range): <0.2 for $S_I(-1,\bar{K})$; <0.02 for $S_I(-2,\bar{K})$; <0.01 for $S_I(-3,\bar{K})$.
[b]The sum-rule values from Ref. [15] are for $K(\theta)$ instead of $\bar{K}$.
[c]The values in parentheses for $\bar{K}^2 > 5.6$ a.u. are equal to $N\bar{K}^{2l}$.

TABLE III. Optical sums.

Sum	This work[a]	Ref. [15]	Ref. [53]	Ref. [54]	Ref. [55]
$S(0)$	14.0[b]	14.0[b]	14.0[b]	13.67	
$S(-1)$	4.85	4.8	4.742	4.61	
$S(-2)$	2.93	2.95	2.935	2.919	2.693,2.859
$S(-3)$	2.17	2.2	2.226		

[a]Uncertainties are the same as those indicated in a footnote in Table II.
[b]Forced to match the theoretical value.

of the correlation energy empirically estimated by Wilson and Silver [59] by use of a wave function with 169,650 configurations using a Slater function basis. Although in the $\bar{K}$ range up to 0.8 a.u. the results from Ref. [56] are in good agreement with ours, their results lie between the unscaled and scaled CI curves reported by Breitenstein, Mayer, and Schweig [35] in the $\bar{K}$ range that extends from 0.8 to 2.5 a.u., with their maximum value located nearly at 1.45 a.u. Our maximum for the $[\Delta S_I(\bar{K})]_{\rm corr}$ curve occurs at a higher value of $\bar{K}$, near 1.7 a.u. It is also worth noting that their values above $\bar{K}=2.8$ a.u. are in excellent agreement with our results.

As a check on the constant K correction we repeated our initial normalization of the data using the full energy-loss range (5–850 eV) with a Bethe-sum-rule value of 14. The ratio of the normalization factors, α_{10}/α_{14}, is plotted in Fig. 7 as a function of $\bar{K}$. If the constant angle to constant momentum transfer correction were large we would expect this ratio to vary strongly as a function of K since as can be seen from Fig. 3 the correction is much more serious at small angles than at large ones. The nearly constant value for this ratio with K adds additional evidence supporting a small correction.

In Fig. 8, our results for $[\Delta S_I(\bar{K})]_{\rm corr}$ are reproduced and fitted with a Gaussian-like function

$$y(\bar{K})=(\bar{K}/C)^A\exp[-(\bar{K}-C)^2/2B^2] \tag{48}$$

with $A=1.669$, $B=0.811$, and $C=1.099$. A lower bound is also shown in this plot to indicate the experimental limits for $\Delta S_I(\bar{K})$ for a straight line background with zero slope which is scaled to the value of the last experimental data point.

Equation (48) with the values for A, B, and C given above has been used in the calculation of the difference function

$$\Delta P(r_{12})=\{[P_0(r_{12})]_{\rm expt}-[P_0^{\rm cl}(r_{12})]_{\rm expt}\}+\{[P_0(r_{12})]_{\rm HF}-[P_0^{\rm cl}(r_{12})]_{\rm HF}\} \tag{49}$$

which was obtained by Fourier transformation of the $[\Delta S_I(\bar{K})]_{\rm corr}$ function. A $\Delta P(r_{12})$ versus r_{12} plot for molecular nitrogen is shown for the first time by the dotted line in Fig. 9. The shape of such a curve is similar to those published by Peixoto, Bunge, and Bonham [60] for He and Ne atoms by comparing theoretical results of $P(r_{ij})$ computed with CI and HF wave functions. Also in

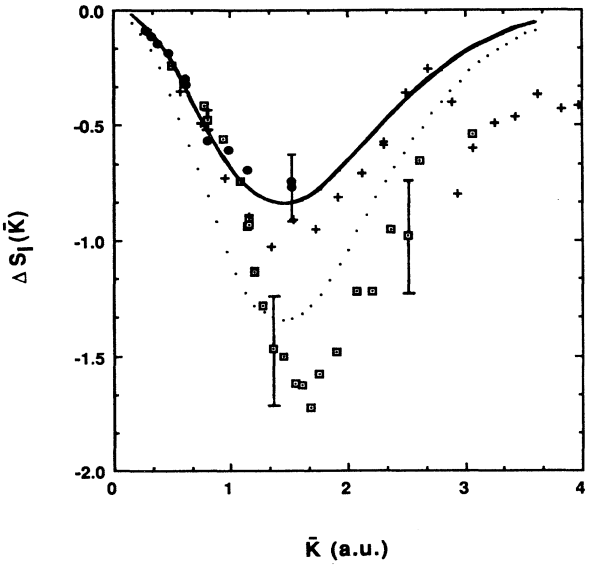

FIG. 6. Comparison of $\Delta S_I(\bar{K})$ as a function of $\bar{K}$ for various experiments. □□□, this work; · · ·, extrapolated theory of Ref. [35]; ——, theory of Ref. [35]; ●●●, experimental results from Ref. [15]; + + +, experimental results from Ref. [56].

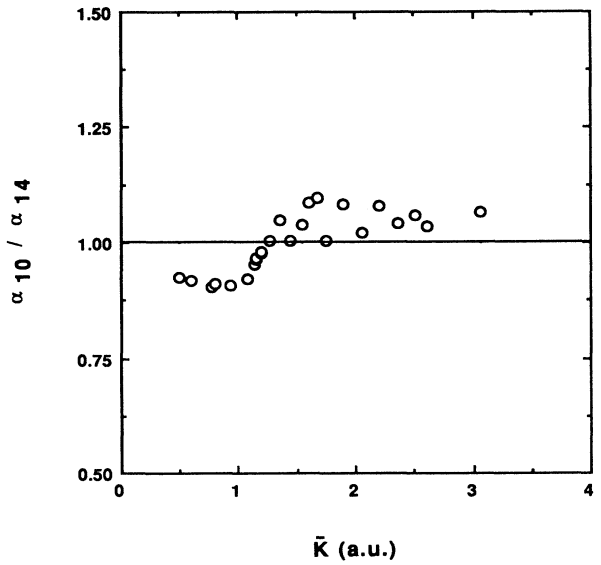

FIG. 7. The ratio of the absolute scale normalizing constant for normalization based on the valence shell to normalization based on the complete spectrum.

TABLE IV. Global properties of the x-ray incoherent scattering factor.

Property	Experimental value	Theoretical value
$\langle r_1 r_2 \cos\theta_{12} \rangle$	-23.1 ± 0.7[a]	-19.72[a,b]
$\cos\theta_c$	-0.612 ± 0.02[a]	-0.530[a,b]
$\int d\mathbf{r} \langle \rho(r)^2 \rangle$		101.36[c]
$\bar{h}(0)$	1401.5 ± 2	1405.2
$\Delta\bar{h}(0)$[d]	-3.7 ± 1	

[a] $\langle r^2 \rangle$ value used was obtained from Ref. [29].
[b] Using $S_I(\bar{K})_{\rm HF}$ from Ref. [34].
[c] Using elastic intensities $I^{\rm XR}_{\rm HF}$ from Ref. [34].
[d] Assumed that $\int d\mathbf{r}\, \Delta[\langle \rho(\mathbf{r})^2 \rangle] \approx 0$.

Fig. 9, the difference between the electron pair correlation function and its classical counterpart $[P_0(r_{12}) - P_0^{\rm cl}(r_{12})]$ as a function of r_{12} is also presented for the first time. These data were generated by Fourier transformation of the quantity $S_I(\bar{K}) - N$. The open circles represent the experimental pair correlation while the full circles indicate the HF values. Smoothed $[S_I(\bar{K})]_{\rm expt}$ data in the $\bar{K}$ range from 3 to 38 a.u. obtained through the relation $[S_I(\bar{K})]_{\rm expt} = [\Delta S_I(\bar{K})]_{\rm corr} + [S_I(\bar{K})]_{\rm HF}$ were used in the Fourier transform. The last three values of $[S_I(\bar{K})]_{\rm HF}$ reported in Ref. [34] have been employed in the preparation of an $S(K) - N$ versus $1/K^4$ plot which was used to estimate $[S_I(\bar{K})]_{\rm HF}$ values not available for $\bar{K} > 24$ a.u. As can be seen, electron-correlation effects, observable through the experimental results, shift the second minimum, which characterizes correlation effects involving valence-shell electrons, to a higher value of r_{12} (≈ 2.2 a.u.). This is very close to the equilibrium bond length ($r_e \approx 2.07$ a.u.) for N_2 [61].

In Table IV the global properties derived from $S_I(\bar{K})$ are presented. In the determination of $\langle r_1 r_2 \cos\theta_{12} \rangle$ the value for $\langle r^2 \rangle = 37.2$ has been obtained from small-angle elastic electron-scattering measurements [29]. The quantity $\cos\theta_c = \langle r_1 r_2 \cos\theta_{12} \rangle / \langle r^2 \rangle$ may be taken as the definition of a correlation angle after Krause, Morgan, and Berry [30]. When using the experimental values of Zeiss *et al.* [53] for $\langle r^2 \rangle + \langle \mathbf{r}_1 \cdot \mathbf{r}_2 \rangle$ and magnetic susceptibility measurements [29] for $\langle r^2 \rangle$ one obtains $\theta_c \approx 129°$ while using electron-scattering data from Ref. [29] one obtains $\theta_c \approx 128°$, which are in very good agreement with the value that can be derived from this work (also using $\langle r^2 \rangle$ from Ref. [29]), $\theta_c \approx 128°$. Numerical Hartree-Fock values yield $\theta_c \approx 122°$ which gives a correlation effect on the order of 5% in θ_c.

Values of $\bar{h}(0)$ have been obtained by use of Eq. (18). The last term on the right-hand side in that equation, assumed to be insensitive to correlation effects, which as we

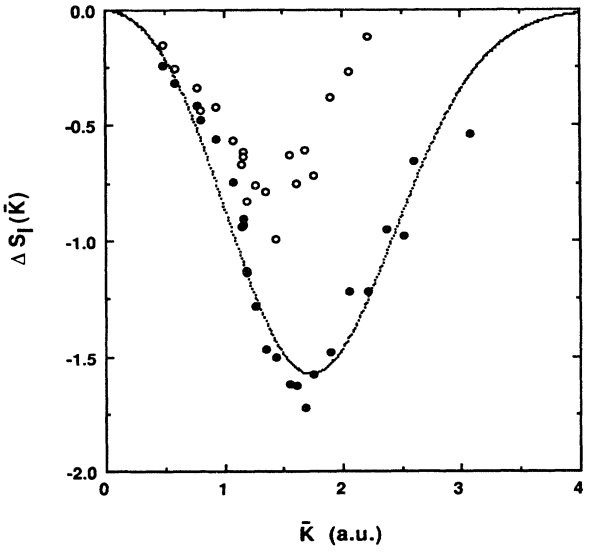

FIG. 8. The effect of the possible existence of a constant background on the $\Delta S_I(\bar{K})$ function. ●●●, experimental points; ···, fitted curve [see Eq. (48) in text]; ○○○, assumed constant background equal to the GOS value at $E = 850$ eV.

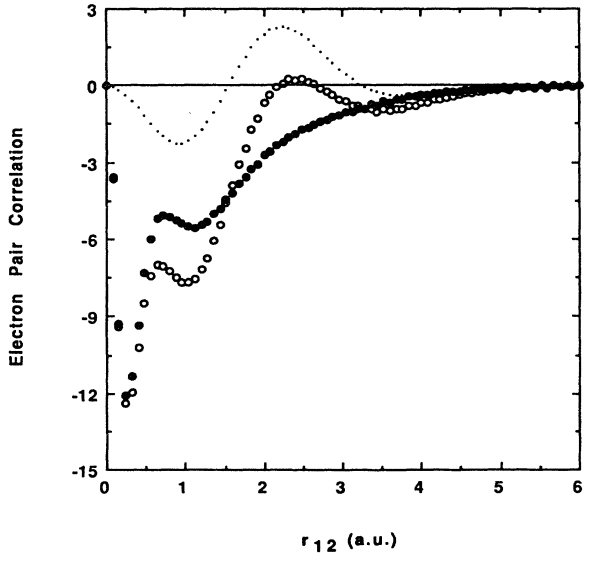

FIG. 9. Electron pair correlation difference functions obtained by Fourier transform of $S_I(\bar{K}) - N$: ●●●, $[P_0(r_{12})]_{\rm HF} - [P_0^{\rm cl}(r_{12})]_{\rm HF}$; ○○○, $[P_0(r_{12})]_{\rm expt} - [P_0^{\rm cl}(r_{12})]_{\rm expt}$; ···, $\Delta P(r_{12}) = \{[P_0(r_{12})]_{\rm expt} - [P_0^{\rm cl}(r_{12})]_{\rm expt}\} - \{[P_0(r_{12})]_{\rm HF} - [P_0^{\rm cl}(r_{12})]_{\rm HF}\}$.

TABLE V. Potential energies.

$\Delta V_{ee}-\Delta V_{ee}^{cl}$	$-27\pm3-3$ eV[a]
	-20.7 eV[b]
ΔV_{ee}^{cl}	$+9.8$ eV[b]
$\Delta V_{en}+\Delta V_{ee}^{cl}$	-10.8 eV[c]
E_c	-16 eV[b,c]
	$-19\pm2-2$ eV[a-c]
	-15 eV[d]
ΔV_{ee}	$-17\pm2-2$ eV[a,b]
	-11 eV[b]
ΔV_{en}	-21 eV[b,c]

[a]Present experiment.
[b]Reference [35]; estimate from 50–55 % CI.
[c]Reference [58]; estimate from 61% CI.
[d]Reference [62]; estimate from 88% CI.

show below may be an unwarranted assumption, has been estimated theoretically by [34,62]

$$\int d\mathbf{r}\langle\rho(\mathbf{r})^2\rangle=\frac{1}{(2\pi)^3}\int d\mathbf{K}|F(\mathbf{K})|^2$$
$$=\frac{1}{2\pi^2}\int_0^\infty d\bar{K}\,\bar{K}^2 I_{HF}^{XR}(\bar{K}) \quad (50)$$

where $I_{HF}^{XR}(\bar{K})$ values were taken from Epstein and Stewart [34]. In the determination of $\bar{h}(0)$ as well as $\Delta\bar{h}(0)$ the integrals over $\bar{K}$ were performed up to $\bar{K}_{max}=4$ a.u., covering the whole range indicated in Fig. 8.

In Table V, the various values for potential energy quantities interpolated from theory and the value obtained in this experiment are given. The correlation energy estimated as $E_c=\Delta V_{ee}/2$ by use of the virial theorem and assuming $\Delta V_{en}=0$ and $\Delta V_{ee}^{cl}=0$ would be -12 ± 3 eV by integrating the area under the Gaussian fit shown in Fig. 8. However, it is possible by use of the available theoretical data to estimate the values of both ΔV_{en} and ΔV_{ee}^{cl} which lead to a very different picture as to the effect of the correlation.

All of the data in Table V taken together suggest that $\frac{2}{3}$ of the correlation effect on the total energy comes through the electron-nuclear attraction, a one-electron quantity, and only about $\frac{1}{3}$ from reduction of the electron-electron repulsion energy. However, because of the weighting by the number of nuclei and the nuclear charges the correlation effect on the one-electron density itself is only about $\frac{1}{7}$ of the effect on the pair correlation density. The error ±3 eV in $\Delta V_{ee}-\Delta V_{ee}^{cl}$ is estimated from the uncertainty of the last data point to which the $1/\bar{K}^4$ tail is matched. The additional -3-eV error estimate is based on the assumption that any background correction is less than 15%. This work strongly suggests that assumptions about small correlation effects on one-electron densities may be unwarranted and must be very carefully considered for each application. This is specially true for the energy where the effect is amplified by the nuclear charge.

Note that in Table V the best theoretical estimate of the correlation energy, -15.0 eV, is from Feller, Boyle, and Davidson [63] who recovered 86% of the estimated total correlation energy (88% of the valence) by use of an extended Gaussian basis set at the self-consistent-field (SCF) and CI levels.

Values of $K(E)$ and $df(K(E),E)/dE$ from 5.8 to 850 eV obtained through this work have been deposited in the Physics Auxiliary Publication Service (PAPS) and are available in microfiche [64].

ACKNOWLEDGMENTS

The authors wish to thank Dr. M. Inokuti for several helpful suggestions and the National Science Foundation for Grant No. PHY-8913096. R.S.B. wishes to thank the Conselho Nacional de Desenvolvimento Científico e Tecnológico–CNPq (Brazil) for support.

[1] T. A. Carlson, *Photoelectron and Auger Spectroscopy* (Plenum, New York, 1975). See Sec. 5.1.2. Note that the case of He is an exception since the final-state wave function is known well.

[2] Two of the rare examples which do show sensitivity to correlation in the ground-state orbital momentum distributions are A.-M. Grisogono, J. Mitroy, R. Pascual, G. Stefani, and E. Weigold, J. Phys. B **21**, 895 (1988); A. O. Bawagan, C. E. Brion, E. R. Davidson, and D. Feller, Chem. Phys. **113**, 19 (1987). A major problem has been the difficulty of obtaining the needed experimental statistical accuracy due to the inherently low count rates of coincidence experiments.

[3] For N_2 the effect of correlation on the Compton profile is less than 2% over the width of the profile and current experimental accuracy is at the 1% level. A. J. Thakkar, J. W. Liu, and W. J. Stevens, Phys. Rev. A **34**, 4695 (1986).

[4] I. E. McCarthy and E. Weigold, Flinders University of South Australia Institute Atomic Studies, Report No. FIAS-R-184, 1987 (unpublished).

[5] Yu. F. Smirnov, V. G. Neudatchin, A. V. Pavlitchenkov, and V. G. Levin, Phys. Lett. **64A**, 31 (1977).

[6] Yu. F. Smirnov, A. V. Pavlitchenkov, V. G. Levin, and V. G. Neudatchin, J. Phys. B **11**, 3587 (1978).

[7] V. G. Levin, V. G. Neudatchin, A. V. Pavlitchenkov, and Yu. F. Smirnov, J. Phys. B **17**, 1525 (1984).

[8] N. P. Yudin, A. V. Pavlitchenkov, and V. G. Neudatchin, Z. Phys. A **320**, 505 (1985).

[9] A. Lahman-Bennani, C. Dupre, and A. Duguet, Phys. Rev. Lett. **63**, 1582 (1989).

[10] J. P. Doering, R. S. Berry, J. H. Moore, and M. A. Coplan, in *Proceedings of the 16th International Conference on the Physics of Electronic and Atomic Collisions, New York, 1989, Abstracts of Contributed Papers,* AIP Conf. Proc. No. 205, edited by A. Dalgarno, R. S. Freund, M. S. Lubell, and T. B. Lucatorto (AIP, New York, 1990), p. 230; A. Lahmam-Bennani, C. Dupre, A. Duguet, and M. Cherid, *ibid.*, p. 235.

[11] J. P. Doering, M. A. Coplan, J. W. Cooper, and J. H. Moore, Phys. Rev. A **41**, 535 (1990).

[12] A description of the early results and theory can be found in A. H. Compton and S. K. Allison, *X-Rays in Theory*

and Experiment, 2nd ed. (Van Nostrand, New York, 1935).
[13] R. A. Bonham and M. Fink, *High Energy Electron Scattering* (Van Nostrand-Reinhold, New York, 1974).
[14] M. Fink, Y. Zhang, and R. A. Bonham, Int. J. Quantum Chem. Symp. **20**, 613 (1986).
[15] S. N. Ketkar and R. A. Bonham, Int. J. Quantum Chem. Symp. **20**, 627 (1986).
[16] T. Iijima and T. Mitsuhashi, Chem. Phys. Lett. **109**, 195 (1984).
[17] F. L. Pilar, *Elementary Quantum Chemistry* (McGraw-Hill, New York, 1968).
[18] To appreciate the difficulties in trying to observe correlation effects in the one-electron density see R. R. Goruganthu and R. A. Bonham, Phys. Rev. A **26**, 1 (1982); J. J. McClelland and M. Fink, *ibid.* **31**, 1328 (1985).
[19] M. Fink and C. Schmiedekamp, J. Chem. Phys. **71**, 4243 (1979).
[20] M. Inokuti, Rev. Mod. Phys. **43**, 297 (1971); M. Inokuti, Y. Itikawa, and J. E. Turner, *ibid.* **50**, 23 (1978).
[21] R. A. Bonham, in *Electron and Magnetization Densities in Molecules and Crystals,* Vol. 48 of *NATO Advanced Study Institute, Series B: Physics,* edited by P. Becker (Plenum, New York, 1980), p. 137.
[22] V. I. Bahzhanov, Teor. Eksp. Khim. **12**, 226 (1976).
[23] I. Shimamura, J. Phys. B **15**, 93 (1982).
[24] R. A. Bonham and G. G. B. de Souza, J. Chem. Phys. **79**, 134 (1983).
[25] T. Iijima, R. A. Bonham, and T. Ando, J. Phys. Chem. **67**, 1472 (1963).
[26] E. B. Wilson, Jr., J. C. Decius, and P. Cross, *Molecular Vibrations: The Theory of Infrared and Raman Vibrational Spectra* (McGraw-Hill, New York, 1935).
[27] R. A. Bonham, J. Phys. Chem. **71**, 856 (1967).
[28] R. A. Bonham and R. S. Barbieri, Quim. Nova **11**, 29 (1988).
[29] R. A. Bonham and M. Fink, Phys. Rev. A **33**, 1569 (1986).
[30] J. L. Krause, J. D. Morgan III, and R. S. Berry, Phys. Rev. A **35**, 3189 (1987).
[31] J. L. Dehmer, M. Inokuti, and R. P. Saxon, Phys. Rev. A **12**, 102 (1975).
[32] V. H. Smith, Jr., Chem. Phys. Lett. **7**, 226 (1970).
[33] A. J. Thakkar and V. H. Smith, Jr., Chem. Phys. Lett. **42**, 476 (1976).
[34] J. Epstein and R. F. Stewart, J. Chem. Phys. **66**, 4057 (1977).
[35] M. Breitenstein, H. Mayer, and A. Schweig, Z. Naturforsch. Teil A **39**, 1208 (1984).
[36] H. Schmoranzer, H. F. Wellenstein, and R. A. Bonham, Rev. Sci. Instrum. **46**, 89 (1975).
[37] H. F. Wellenstein and R. E. Ensman, Rev. Sci. Instrum. **44**, 922 (1973).
[38] F. Sperisen, A. Berdoz, H.-O. Meyer, R. S. Barbieri, and R. A. Bonham, Nucl. Instrum. Methods A **274**, 604 (1989).
[39] H. F. Wellenstein, H. Schmoranzer, R. A. Bonham, T. C. Wong, and J. S. Lee, Rev. Sci. Instrum. **46**, 92 (1975).
[40] R. A. Bonham and C. Tavard, J. Chem. Phys. **39**, 469 (1973).
[41] This correction must be made for all electrostatic analyzers used to measure varying input energies with a fixed width of the entrance slit and was first given by Kollath for a different type of analyzer than the one used here. The necessary modification for a Mollenstedt analyzer can be found in his second paper: R. Kollath, Ann. Phys. (Leipzig) **27**, 721 (1936). See also K. H. Glauker, Z. Phys. **196**, 85 (1966). This correction in our work varies from zero at $E=0$ to 6% of the intensity at $E=1000$ eV.
[42] M. J. Brothers and R. A. Bonham, J. Phys. B **17**, 4235 (1984).
[43] M. Inokuti (private communication).
[44] J. L. Dehmer and D. Dill, J. Chem. Phys. **65**, 5327 (1976).
[45] A. R. P. Rau and U. Fano, Phys. Rev. **162**, 68 (1967).
[46] R. A. Bonham, Chem. Phys. Lett. **18**, 454 (1973).
[47] H. F. Wellenstein and R. A. Bonham, Chem. Phys. Lett. **15**, 530 (1972).
[48] M. Inokuti and M. R. C. McDowell, J. Phys. B **7**, 2382 (1974).
[49] E. H. Darlington, J. Phys. D **8**, 85 (1975).
[50] R. A. Bonham, in *Momentum Wave Functions—1976 (Indiana University),* Proceedings of the Workshop/Seminar on Momentum Wave Function Determination in Atomic, Molecular, and Nuclear Systems, edited by D. W. Devins, AIP Conf. Proc. No. 36 (AIP, New York, 1977).
[51] H. F. Wellenstein, R. A. Bonham, and R. C. Ulsh, Phys. Rev. A **8**, 304 (1973).
[52] R. A. Bonham and H. F. Wellenstein, J. Appl. Phys. **44**, 2631 (1973).
[53] G. D. Zeiss, W. J. Meath, J. C. F. MacDonald, and D. J. Dawson, Can. J. Phys. **55**, 2080 (1977).
[54] J. Berkowitz, *Photoabsorption, Photoionization and Photoelectron Spectroscopy* (Academic, New York, 1979).
[55] M. A. Spackman, J. Chem. Phys. **94**, 1288 (1991).
[56] Y. Zhang, A. W. Ross, and M. Fink, Z. Phys. D **18**, 163 (1991).
[57] See Ref. [35] and also M. Breitenstein, A. Endesfelder, H. Meyer, and A. Schweig, Chem. Phys. Lett. **108**, 430 (1984).
[58] J. W. Liu, G. C. Lie, and B. Liu, J. Phys. B **20**, 2853 (1987).
[59] S. Wilson and D. M. Silver, J. Chem. Phys. **67**, 1689 (1977).
[60] E. M. A. Peixoto, C. F. Bunge, and R. A. Bonham, Phys. Rev. **181**, 322 (1969).
[61] See, for example, *American Institute of Physics Handbook,* edited by D. E. Gray, 3rd ed. (McGraw-Hill, New York, 1982).
[62] R. A. Bonham and W. Weyrich, J. Braz. Chem. Soc. **1**, 7 (1990).
[63] D. Feller, C. M. Boyle, and E. R. Davidson, J. Chem. Phys. **86**, 3424 (1987).
[64] See AIP document No. PAPS PLRAA-44-7361-48 for 48 pages of experimental data. Order by PAPS number and journal reference from American Institute of Physics, Physics Auxiliary Publication Service, 335 East 45th Street, New York, NY, 10017. The prepaid price is $1.50 for each microfiche (98 pages) or $5.00 for photocopies of up to 30 pages, and $0.15 for each additional page over 30 pages. Airmail additional. Make checks payable to the American Institute of Physics.